PAPER

Directional Chiral Optical Emission by Electron-Beam-Excited Nano-Antenna

To cite this article: Xiang Xiong *et al* 2023 *Chinese Phys. Lett.* **40** 017801

Directional Chiral Optical Emission by Electron-Beam-Excited Nano-Antenna

Xiang Xiong(熊翔)[1], Zhao-Yuan Zeng(曾昭源)[1], Ruwen Peng(彭茹雯)[1*], and Mu Wang(王牧)[1,2*]

[1]*National Laboratory of Solid State Microstructures, School of Physics, and Collaborative Innovation Center of Advanced Microstructures, Nanjing University, Nanjing 210093, China*
[2]*American Physical Society, 100 Motor Parkway, Hauppauge, New York 11778, USA*

(Received 19 October 2022; accepted manuscript online 25 November 2022)

Manipulating directional chiral optical emissions on a nanometer scale is significant for material science research. The electron-beam-excited nanoantenna provides a favorable platform to tune optical emissions at the deep subwavelength scale. Here we present an L-shaped electron-beam-excited nanoantenna (LENA) with two identical orthogonal arms. By selecting different electron-beam impacting sites on the LENA, either the left-handed circularly polarized (LCP) or the right-handed circularly polarized (RCP) emission can be excited. The LCP and RCP emissions possess different emission directionality, and the emission wavelength depends on the arm length of the LENA. Further, we show a combined nanoantenna with two LENAs of different arm lengths. Induced by the electron beam, LCP and RCP lights emit simultaneously from the nanoantenna with different wavelengths to different directions. This approach is suggested to be informative for investigating electron-photon interaction and electron-beam spectroscopy in nanophotonics.

DOI: 10.1088/0256-307X/40/1/017801

Utilization of circularly polarized (CP) light is one of the most traditional topics in optical research.[1] Various technologies based on CP light have played essential roles in chemical identification,[2] nanoparticle manipulation,[3] quantum communication,[4] and so on. In many optical devices, CP light is generated by passing linearly polarized (LP) light through a quarter waveplate.[5] A conventional waveplate is made of a birefringence crystalline plate cutting along a specific crystallography orientation. The optical functionality of the waveplate depends on both the material birefringence and the crystal plate thickness. The waveplate must be thick enough for conventional materials to accumulate the required optical path difference between the o-ray and e-ray.[6] However, with the development of integrated optics and modern on-chip photonics, conventional waveplates cannot meet the demanding integration requirements.

Recently developed metasurfaces provide ultra-thin and lightweight solutions to replace conventional crystalline waveplates.[7] Depending on the specific design, left-handed circularly polarized (LCP) or/and right-handed circularly polarized (RCP) lights can be generated from LP,[8–10] CP,[11,12] and even-unpolarized[13] incidence. By exciting an individual subwavelength nanoantenna with an electron beam, optical emissions can be effectively generated on subwavelength scales.[14,15] So far, polarization-resolved radiation,[16–18] angular emission,[19,20] and breathing plasmon modes[21,22] have been realized with nanoantennas. Among these previous studies, chiral emissions excited by electron beams from nanoantennas are particularly attractive.[16–18,23–25] CP lights of different handedness can be obtained by designing the nanoantenna structure and the excitation site. However, generating and switching CP lights with an individual nanoantenna remains challenging. On the other hand, generating CP light on a nanoscale would be beneficial for subwavelength polarization optics.[26] In this Letter, we demonstrate the design of an L-shaped electron-beam-excited nanoantenna (LENA). By selecting different impacting positions on the LENA, LCP and RCP radiations can be alternatively or simultaneously generated. We further build a combined nanoantenna with two LENAs of different arm lengths. The combined nanoantenna can generate CP lights with opposite chiralities and emission directions at two different wavelengths. Since it is critical to realize polarization state switching in a highly compact space,[27,28] our design provides an effective scheme of CP state switching on the nanometer scale.

The schematic diagram of the LENA is shown in Fig. 1(a). The LENA is a gold structure on the silicon substrate with a 100 nm SiO_2 layer. Two orthogonal arms of the gold structure form an L-pattern. A Cartesian coordinate is established with one arm pointing to the x-direction (x-arm) and the other pointing to the y-direction (y-arm). An electron beam shines along the $-z$-direction to the LENA, and the incident site can be selected. As shown in Fig. 1(b), we establish a spherical coordinate (ϕ, θ) to characterize the angular profiles of the emission directionality. The LENA locates at the origin of the spherical coordinate. The direction of the azimuthal angle $\phi = 0^\circ$ is set along the bisector of the x- and y-arms, whereas the direction of the zenithal angle $\theta = 0^\circ$ is along the z-axis.

The finite-difference time-domain (FDTD) simulation is applied, and the optical parameters of Au, Si, and SiO_2 are all from Palik.[29] The simulated electron beam is represented by a series of closely placed electric dipoles along the electron trajectory.[30] To calculate the optical emissions, in our simulation, the electron beam mov-

*Corresponding authors. Email: rwpeng@nju.edu.cn; muwang@nju.edu.cn

ing in $-z$-direction is treated as a linear current density $\boldsymbol{J}(\omega, \boldsymbol{r}) = ev\exp(\frac{-i\omega z}{v})\delta(x-x_0)\delta(y-y_0)\boldsymbol{n}_z$, where e is the electron charge, v is the velocity of electrons, (x_0, y_0) is the excitation position of the electron beam, and $\boldsymbol{n}_z$ is the unit vector in the z-direction.[31] The electron velocity v is adjusted by the temporal phase delay $(-z/v)$. In the simulation, v is set as $0.34c$ (c is the velocity of light in the vacuum), corresponding to 30 keV of the beam current energy.[31] This arrangement is due to the fact that 30 keV ($v = 0.34c$) is the typical electron energy used in cathodoluminescence spectroscopy in a scanning electron microscope.[14] We calculate the total emission intensity I_{total} for different impacting positions by integrating the Poynting vector in the upper hemisphere of the sphere coordinate as

$$I_{\text{total}} = \frac{1}{2}\int\sqrt{\frac{\varepsilon_0}{\mu_0}}\left(|E_\theta|^2 + |E_\phi|^2\right)ds, \tag{1}$$

where E_ϕ and E_θ are the electric fields along ϕ- and θ-directions in the sphere coordinates, respectively.[16] In our simulation, a reference simulation (without the LENA and substrate) was carried out to subtract the background signal created by the electron beam that could obscure the signal from the nanoantenna.

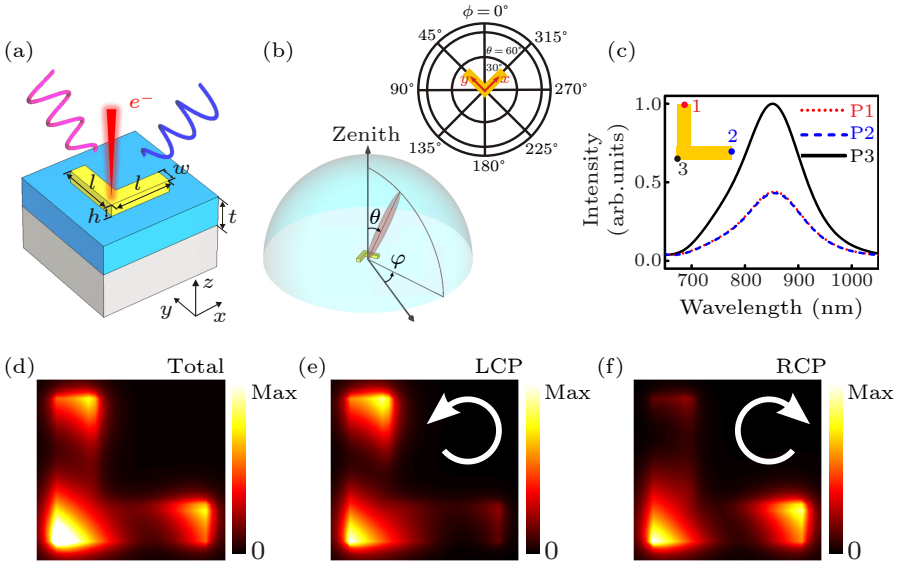

Fig. 1. (a) Schematic diagram of the LENA with $l = 200$ nm, $h = 40$ nm, $w = 50$ nm, and $t = 100$ nm. (b) The spherical coordinate characterizes the angular directionality of the optical emission. The inset at the up-right corner shows the relative position of the Cartesian coordinate and the sphere coordinate. (c) The total emission intensities for different impacting positions versus the wavelength. The spatially resolved mappings of (d) the total, (e) the LCP, and (f) the RCP emission intensities at the wavelength of 850 nm.

As shown in Fig. 1(c), the two arm ends and the connecting corner of the L-pattern are selected as the incident sites. Intensity peaks occur at the same wavelength of 850 nm, and the emission intensity for the electron beam impacting the corner is about twice that on the arm ends. Due to the structural symmetry of the L-pattern, emission intensities are identical when the incidence site locates at either x- or y-arm ends.

To investigate the chiral property of the optical radiation, we derive the LCP and RCP emission intensities (I_{LCP} and I_{RCP}) by integrating the corresponding electric fields in the upper hemisphere as

$$I_{\text{LCP}} = \frac{1}{4}\int\sqrt{\frac{\varepsilon_0}{\mu_0}}\left(|\boldsymbol{E}_\theta - i\boldsymbol{E}_\phi|^2\right)ds, \tag{2}$$

$$I_{\text{RCP}} = \frac{1}{4}\int\sqrt{\frac{\varepsilon_0}{\mu_0}}\left(|\boldsymbol{E}_\theta + i\boldsymbol{E}_\phi|^2\right)ds. \tag{3}$$

We plot the spatially resolved mappings of the emission intensities at the wavelength of 850 nm in Figs. 1(d)–1(f). The brightness distributions reveal the normalized intensities of the total, the LCP, and the RCP emissions at different electron beam incidence sites. Figure 1(d) shows that total emissions are efficiently generated when the electron beam shines on the two arm ends and the connecting corner of the LENA. Figure 1(e) shows that when the electron beam shines on the y-arm end and the connecting corner of the LENA, the LCP emission can be efficiently excited. The electron beam does not induce obvious LCP emission at the x-arm end. The situation for the RCP optical emission is just the opposite. When the electron beam focuses on the x-arm end and the corner of the LENA, the RCP emission can be efficiently excited. Similarly, the electron beam does not induce obvious RCP emission when focused at the y-arm end. Comparing Figs. 1(e) and 1(f), we can find that the strong LCP and RCP emissions are alternatively induced when the electron beam selectively shines on the y-arm end or the x-arm end. The effective LCP and RCP emissions are simultaneously generated when the electron beam focuses on the corner of the L-shaped nanoantenna.

We further explore the angular directionality of the chiral emissions for different electron-beam incidence sites.

As shown in Fig. 2(a), the election beam focuses on the y-arm end, and only the LCP emission is effectively excited. Figure 2(b) shows the electric field distributions of $|E_z|$ at 850 nm. When the electron beam focuses on the y-arm end of the LENA, field enhancement can be observed in both x- and y-arm areas. The field enhancement in the y-arm area is stronger than that in the x-arm. The angular radiation directions are calculated for LCP and RCP emissions, respectively. Figure 2(c) shows that the LCP emission locates in the right half of the upper angular hemisphere, specifically, ϕ ranges from 225° to 315°. The RCP emission intensity is much weaker in all angular directions. To characterize the difference in polarization states, we define the parameter chirality as $(I_{\mathrm{LCP}}-I_{\mathrm{RCP}})/(I_{\mathrm{LCP}}+I_{\mathrm{RCP}})$.[16] The chirality as a function of solid angles is shown in Fig. 2(d). For most of the angular range in the hemisphere, the chirality is close to 1. A directional LCP optical emission is obtained when the electron beam focuses on the y-arm end of the LENA. In Figs. 2(e)–2(h) the incident site is located on the x-arm end, and the result is the opposite. The electric field enhancement in the x-arm area is stronger than that in the y-arm. Directional RCP emission is obtained, and the RCP emission occurs in the angular range of ϕ from 45° to 135°. In Figs. 2(i)–2(l), we move the incident site to the corner of the LENA. Equal-intensity LCP and RCP lights are generated, and the electric field enhancement in the x- and y-arm areas are the same. In Figs. 2(k), a distinct splitting of LCP and RCP emissions can be observed. The LCP optical emission locates in the right half of the angular hemisphere, with ϕ ranging from 225° to 315°. In contrast, the RCP emission occurs when ϕ varies from 45° to 135°, which is in the left half of the angular hemisphere. In Fig. 2(l), the chirality is negative and positive in the left and right halves of the angular hemisphere, respectively, confirming the spatial separation of the oppositely handed radiations.

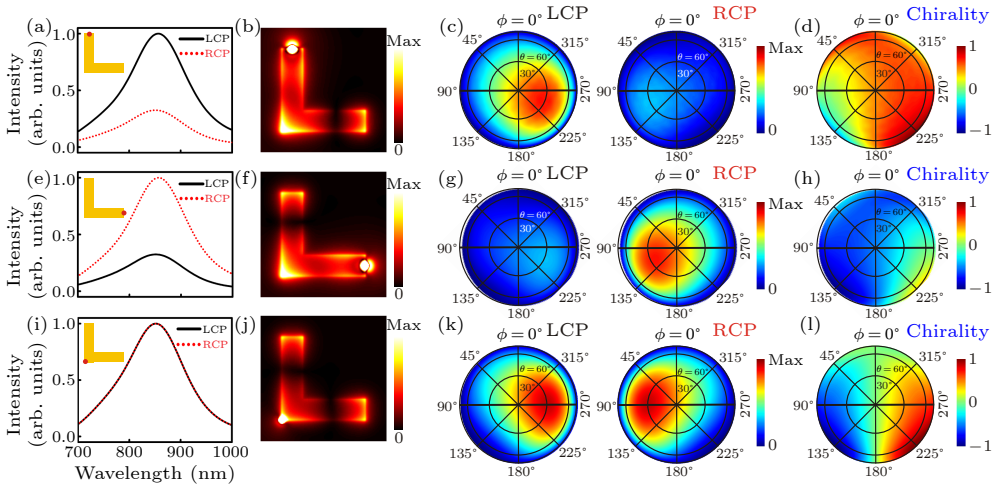

Fig. 2. The LCP and RCP emission intensities versus the wavelength, the electric field distributions of $|E_z|$, the LCP and RCP emission intensities, and the chirality as a function of solid angles. The incident site for (a)–(d) is at the y-arm end, for (e)–(h) is at the x-arm end, and for (i)–(l) is at the connecting corner of the LENA. The cross-section of $|E_z|$ distributions is 5 nm above the nanoantenna.

Interestingly, with an individual nanoantenna, radiations of opposite chiralities can be excited and spatially separated into different directions. We further study the relationship between the radiation peak wavelength and the arm length of the LENA. We select the incident site at the LENA corner and different arm lengths while the rest of the structural parameters remain unchanged. As illustrated in Fig. 3(a), the LCP and RCP emissions have equal intensity, and the peaks appear at the wavelength of 745 nm when the arm length is 160 nm. As shown in Figs. 3(b)–3(d), by changing the arm length to 180 nm, 220 nm, and 240 nm, respectively, the peak wavelength shifts to 785 nm, 900 nm, and 940 nm accordingly. The electric field distributions of $|E_z|$ show that changing the arm length of the antenna does not affect the symmetry of the electromagnetic mode. The angular patterns of the oppositely handed radiations and the chirality as a function of solid angles are also calculated for different arm lengths. The calculated results show that by changing the LENA arm length, we can modulate the peak wavelength of the directional chiral emissions. The equal-intensity LCP and RCP emissions can keep the spatial separation during the wavelength modulation. During the changing of the geometric parameters of the LENA, the LCP and RCP emissions remain efficiently excited, and the oppositely handed radiations keep their spatial separation.

We further build a combined nanoantenna by placing two LENAs contacting each other with their corners. As shown in Fig. 4(a), the combined nanoantenna is constructed with a larger LENA with an arm length $l_1 = 240$ nm and a smaller LENA with an arm length $l_2 = 160$ nm. The arms of the larger LENA point to x and y directions, while the arms of the smaller LENA point to $-x$ and $-y$ directions. The electron beam impacts the connecting corners of the two LENAs. The intensities of the total, the LCP, and the RCP emissions show that two radiation peaks appear at 670 nm and 865 nm. Figures 4(c) and 4(d) show the electric field distributions of $|E_z|$ at these two wavelengths. It can be seen that, at the wavelength of 670 nm, an obvious electric field en-

hancement appears in the area of the smaller LENA. In comparison, at the wavelength of 865 nm, the electric field enhancement appears in the area of the larger LENA. The angular patterns of the LCP and RCP emissions at the two peak wavelengths are illustrated in Figs. 4(e) and 4(f). Figure 4(e) shows that at 670 nm, LCP emission occurs with ϕ varying from 0° to 90°, while the RCP emission occurs with ϕ in the range from 270° to 360°. However, as shown in Fig. 4(f), at 865 nm LCP emission occurs with ϕ in the range from 180° to 270°, whereas RCP emission occurs with ϕ in the range from 90° to 180°. By driving the combined nanoantenna with an electron beam, LCP and RCP emissions can be excited concurrently at shorter and longer wavelengths. The four chiral emissions occur and emit in different angular directions.

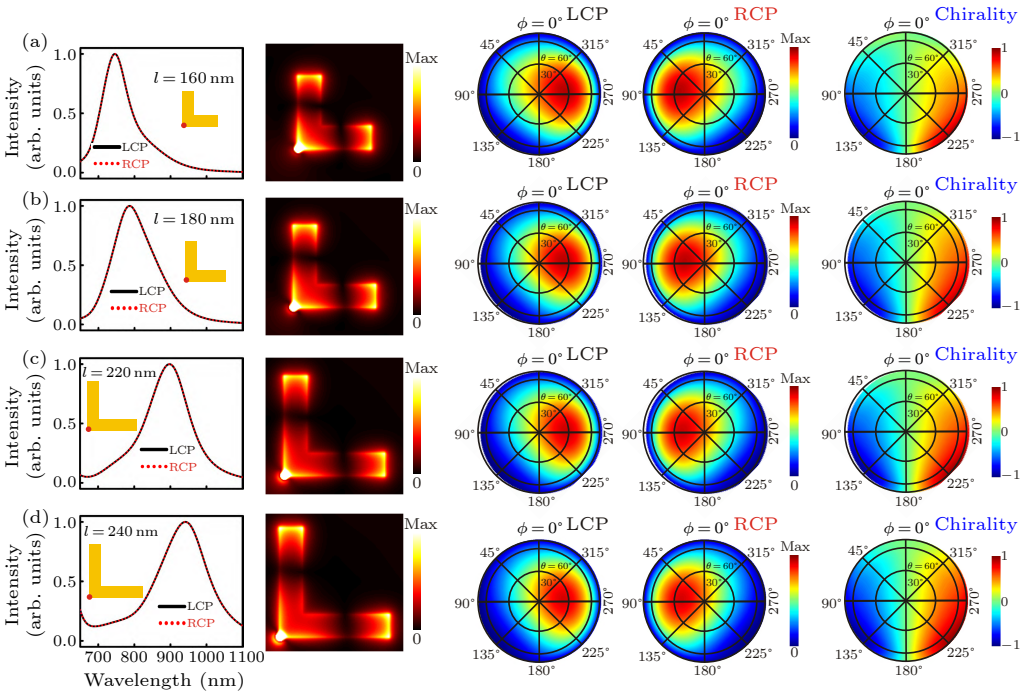

Fig. 3. The LCP and RCP emission intensities versus the wavelength, and the electric field distributions of $|E_z|$, the angular directions of the LCP and RCP emission and the chirality as a function of solid angles, for different arm lengths: (a) $l = 160$ nm, (b) $l = 180$ nm, (c) $l = 220$ nm, (d) $l = 240$ nm. The cross section of $|E_z|$ distributions is 5 nm above the nanoantenna.

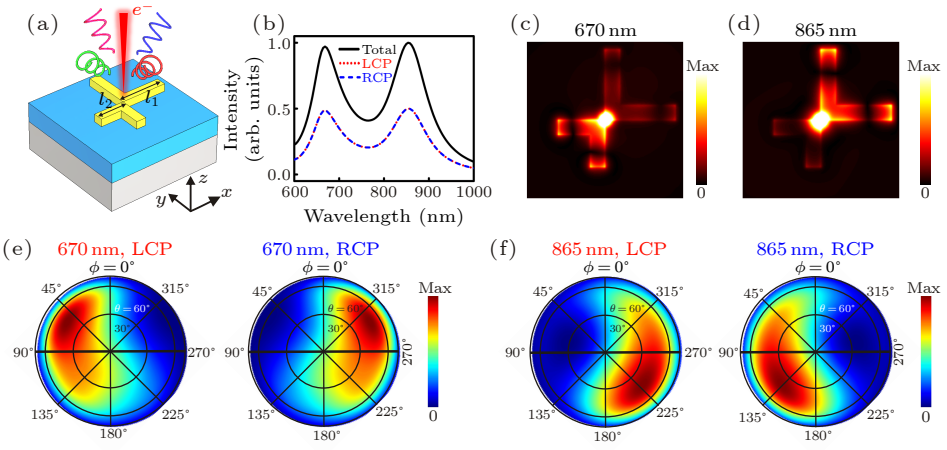

Fig. 4. (a) The schematic diagram of the combined nanoantenna. (b) The total, LCP, and RCP emission intensities versus the wavelength. The electric field distributions of $|E_z|$ at (c) 670 nm and (d) 865 nm. The cross-sections (c) and (d) are 5 nm above the nanoantenna. The intensities of the chiral emissions as a function of solid angles for the LCP and RCP emissions (e) at 670 nm and (f) at 865 nm.

The above results indicate that for the electron-beam-excited nanoantennas, the optical properties of the emissions are determined by both the antenna structure and the position of the electron beam incidence. When the electron beam impacts at the corner of the LENA or the connecting corners of two LENAs in the combined nanoantenna, the mirror symmetry of the excitation site and the equal arm length of the L-shaped antenna guarantee the

symmetric angular distributions and identical intensity of the LCP and RCP emissions simultaneously. The symmetry is broken when the electron beam is focused at the end of the x- or y-arm of the L-shaped antenna. The asymmetric excitation site leads to the asymmetric electromagnetic resonance mode on the x- and y-arms of the LENA, resulting in either LCP or RCP emission. Changing the structural parameters of the LENA arms can modulate the optical emission wavelength. Compared with the arm length, tuning the width or the thickness of the LENA arms is less efficient in modulating the wavelength of the chiral emissions. The simulations in Fig. 3 show that a 20% change in the LENA arm length can achieve about 100 nm shift of the radiation wavelength. In contrast, to realize the same wavelength shift, the arm width or arm thickness has to be changed by more than 50%. It is noteworthy that the L-shaped structure is often used as the meta-atom in designing metamaterial and metasurface.[9] Just as discussed in previous studies,[8–10,32] by judiciously selecting the geometrical size and the symmetry of each L-shaped antenna and by carefully designing the lattice parameters, we can accurately control the response wavelength, the output polarization states, the number of output light beams and the propagation direction of each light beam.

To summarize, we have studied the emission behavior of an L-shaped electron-beam-excited nanoantenna by simulation. The LCP and RCP emissions can be alternatively or simultaneously excited by selecting different electron incident sites on the antenna. A combined nanoantenna is constructed with two different-sized nanoantennas, leading to LCP and RCP emitting in different directions with different wavelengths. It is expected that these effects are enlightening to study electron-photon interaction and electron-beam spectroscopy in nanoplasmonics.

Acknowledgments. This work was supported by the National Key R&D Program of China (Grant No. 2020YFA0211300), and the National Natural Science Foundation of China (Grant Nos. 11974177, 61975078, and 12234010).

References

[1] Kliger D S, Lewis J W, and Randall C E 1990 *Polarized Light in Optics and Spectroscopy* (Boston: Academic Press)
[2] Imai Y, Nakano Y, Kawai T, and Yuasa J 2018 *Angew. Chem. Int. Ed.* **57** 8973
[3] La P A and Wang M D 2004 *Phys. Rev. Lett.* **92** 190801
[4] Gisin N and Thew R 2007 *Nat. Photon.* **1** 165
[5] Hecht E 2017 *Optics* (Boston: Pearson Education, Inc.)
[6] Born M, Wolf E, and Bhatia A B 2019 *Principles of Optics: Electromagnetic Theory of Propagation, Interference, and Diffraction of Light* (Cambridge: Cambridge University Press)
[7] Yu N F, Aieta F, Genevet P, Kats M A, Gaburro Z, and Capasso F 2012 *Nano Lett.* **12** 6328
[8] Gao Y J, Xiong X, Wang Z H, Chen F, Peng R W, and Wang M 2020 *Phys. Rev. X* **10** 031035
[9] Jiang S C, Xiong X, Hu Y S, Hu Y H, Ma G B, Peng R W, Sun C, and Wang M 2014 *Phys. Rev. X* **4** 021026
[10] Jiang S C, Xiong X, Sarriugarte P, Jiang S W, Yin X B, Wang Y, Peng R W, Wu D, Hillenbrand R, Zhang X, and Wang M 2013 *Phys. Rev. B* **88** 161104
[11] Maguid E, Yulevich I, Veksler D, Kleiner V, Brongersma M L, and Hasman E 2016 *Science* **352** 1202
[12] Wang Z J, Jia H, Yao K, Cai W S, Chen H S, and Liu Y M 2016 *ACS Photon.* **3** 2096
[13] Kim M, Lee D, and Rho J 2021 *Laser Photon. Rev.* **15** 2100138
[14] Polman A, Kociak M, and de Abajo F J G 2019 *Nat. Mater.* **18** 1158
[15] Fung K H, Kumar A, and Fang N X 2014 *Phys. Rev. B* **89** 045408
[16] Chi C, Jiang Q, Liu Z X, Zheng L H, Jiang M L, Zhang H, Lin F, Shen B, and Fang Z Y 2021 *Sci. Adv.* **7** eabf8011
[17] Matsukata T, de Abajo F J G, and Sannomiya T 2021 *ACS Nano* **15** 2219
[18] Wang J X, Li G H, Ou K, Yu F L, Chen J, Li Z F, Chen X S, and Lu W 2021 *J. Phys. D* **54** 105105
[19] Mignuzzi S, Mota M, Coenen T, Li Y, Mihai A P, Petrov P K, Oulton R F M, Maier S A, and Sapienza R 2018 *ACS Photon.* **5** 1381
[20] Osorio C I, Coenen T, Brenny B J M, Polman A, and Koenderink A F 2016 *ACS Photon.* **3** 147
[21] Zhao X M, Du C L, Leng R, Li L, Luo W W, Wu W, Xiang Y X, Ren M X, Zhang X Z, Cai W, and Xu J J 2021 *Nanoscale Adv.* **3** 4286
[22] Li L, Zhao D P, Fan J, Huang R, Wu W, Ren M X, Zhang X Z, Cai W, and Xu J J 2020 *J. Opt.* **22** 035003
[23] Asenjo-Garcia A and de Abajo F J G 2014 *Phys. Rev. Lett.* **113** 066102
[24] Harvey T R, Henke J W, Kfir O, Lourenco-Martins H, Feist A, de Abajo F J G, and Ropers C 2020 *Nano Lett.* **20** 4377
[25] Zu S, Han T Y, Jiang M L, Liu Z X, Jiang Q, Lin F, Zhu X, and Fang Z Y 2019 *Nano Lett.* **19** 775
[26] Wang M J, Salut R, Lu H H, Suarez M A, Martin N, and Grosjean T 2019 *Light Sci. Appl.* **8** 76
[27] Ding F, Tang S, and Bozhevolnyi S I 2021 *Adv. Photo. Res.* **2** 2000173
[28] Li J X, Yu P, Cheng H, Liu W W, Li Z C, Xie B Y, Chen S Q, and Tian J G 2016 *Adv. Opt. Mater.* **4** 91
[29] Palik E D 1998 *Handbook of Optical Constants of Solids* (San Diego: Academic Press)
[30] Chaturvedi P, Hsu K H, Kumar A, Fung K H, Mabon J C, and Fang N X 2009 *ACS Nano* **3** 2965
[31] Zheng L H, Liu Z X, Liu D L, Wang X G, Li Y, Jiang M L, Lin F, Zhang H, Shen B, Zhu X, Gong Y J, and Fang Z Y 2021 *Nat. Commun.* **12** 291
[32] Gao Y J, Wang Z, Jiang Y, Peng R W, Wang Z Y, Qi D X, Fan R H, Tang W J, and Wang M 2022 *Phys. Rev. Lett.* **129** 023601